

The role of electrical and thermal contact resistance for Joule breakdown of single-wall carbon nanotubes

Eric Pop

Department of Electrical and Computer Engineering, Micro and Nanotechnology Laboratory,
University of Illinois at Urbana-Champaign, Urbana, IL 61801, USA

E-mail: epop@uiuc.edu

Received 16 December 2007, in final form 13 May 2008

Published 10 June 2008

Online at stacks.iop.org/Nano/19/295202

Abstract

Several data sets for the electrical breakdown in air of single-wall carbon nanotubes (SWNTs) on insulating substrates are collected and analyzed. A *universal* scaling of the Joule breakdown power with nanotube length is found, which appears to be independent of the substrate thermal properties or their thickness. This suggests that the thermal resistances at SWNT–insulator and at SWNT–electrode interfaces govern heat sinking from the nanotube. Analytical models for the breakdown power scaling are presented, providing an intuitive, physical understanding of the breakdown process. The electrical and thermal resistances at the electrode contacts limit the breakdown behavior for sub-micron SWNTs; the breakdown power scales linearly with length for tubes that are microns long, and a minimum breakdown power (~ 0.05 mW) is observed for the intermediate (~ 0.5 μm) length range.

(Some figures in this article are in colour only in the electronic version)

The electrical and thermal behavior of single-wall carbon nanotubes has been intensely studied in recent years [1–6]. Controlled electrical breakdown of SWNTs, i.e. ‘cutting,’ has been used to create electrodes for single-molecule experiments [7, 8], and their breakdown has been noted in the context of field-emission sources [9, 10] and bulk thermogravimetric (TGA) experiments [11, 12]. In-air electrical breakdown of SWNTs supported by an insulating substrate has also been proposed as a selective mechanism for preferentially eliminating metallic nanotubes among semiconducting ones as a bottom-up approach to building SWNT circuits [13, 14].

However, little is known specifically about SWNT device breakdown and reliability at high temperature, and about the role the ubiquitous contacts play in power generation and dissipation. Understanding and controlling the breakdown power (voltage) of nanotubes is also important for selective elimination of metallic among semiconducting SWNTs in electronic circuits. While previous work has developed electrothermally coupled metallic nanotube transport models [1, 15], this manuscript analyzes, for the first time, the specific role

played by the nanotube–electrode contacts in electrical and thermal transport and high-voltage breakdown.

SWNT breakdown voltage data is collected from studies by Seidel *et al* [14] (from here on referred to as the Infineon data set), Maune *et al* [16] (the Caltech data set), Javey *et al* [17] and Pop *et al* [15] (the Stanford data sets). The devices in these various studies share a similar geometric layout, i.e. a single-wall nanotube bridging two metallic contacts on top of an insulating material layer (figure 1(a)). The silicon wafer beneath is used as a back-gate, where necessary, to fully turn on the semiconducting tubes. The top of the nanotube is left uncovered and exposed to the ambient air. Only nanotubes whose complete I – V electrical characteristics were available, up to electrical breakdown, have been used in the present study. Combined, the set of electrically contacted SWNTs considered here covers a wide range of nanotube lengths ($10\text{ nm} < L < 8\text{ }\mu\text{m}$), diameters ($0.8\text{ nm} < d < 3.2\text{ nm}$), and electrical contact resistance ($9\text{ k}\Omega < R_C < 830\text{ k}\Omega$). The physical dimensions are typically obtained from AFM measurements, while the electrical contact resistance (R_C for the two contacts combined) is estimated from the linear portion of the

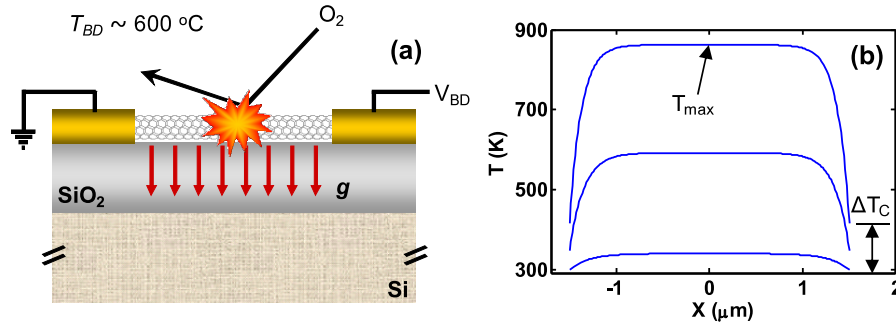


Figure 1. (a) Schematic of oxidation-induced SWNT breakdown, when exposed to air at high applied voltage. The length of the nanotube portion between the contacts is L , the heat conduction into the substrate per unit length is g (red arrows into substrate). (b) Calculated temperature profile for a $3 \mu\text{m}$ long tube at 3, 9 and 15 V bias from bottom to top. Note the peak temperature near the middle of the tube (where breakdowns are confirmed by AFM [17]) and the temperature drop ΔT_C at the contacts.

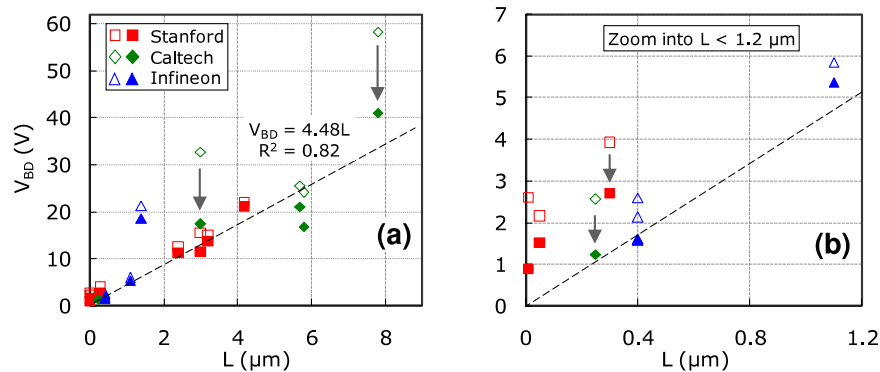


Figure 2. (a) Breakdown voltage versus SWNT length from the Stanford [16, 17], Caltech [15] and Infineon [14] data sets. Empty symbols are before, and solid symbols are after removing the electrical contact resistance drop IR_C (arrows highlight some of the changes). (b) Same data sets, zoomed into the shorter nanotube range.

I - V curve at low bias, and therefore incorporates the quantum contact resistance ($h/4q^2 \approx 6.5 \text{ k}\Omega$).

The mechanism for in-air electrical breakdown of SWNTs is as follows. The voltage applied across the nanotube is raised (and the current typically increases) until the power dissipated is large enough to cause significant self-heating of the SWNT. If the power dissipation is uniform, the peak temperature occurs in the middle of the tube, and once this point reaches the breakdown temperature the nanotube oxidizes (burns) irreversibly. This yields a sharp drop to zero in the I - V curve, and a physical ‘cut’ in the nanotube itself. A cartoon of this process is shown in figure 1(a). Figure 1(b) displays the temperature profiles computed along a $3 \mu\text{m}$ nanotube at various voltages, using the model described in [15]. Breakdown voltages in vacuum or an inert ambient (e.g. Ar) are known to be significantly higher than those in air [7, 18], suggesting this is indeed an oxidation-induced breakdown [19]. In addition, AFM imaging of broken SWNTs [17] shows these cuts occur near the middle of the tube, where the temperature peaks. The breakdown temperature of SWNTs is known to be approximately $T_{BD} \approx 600 \text{ }^\circ\text{C}$ from thermogravimetric (TGA) analysis of bulk samples [11, 12]. A range of $\pm 100 \text{ }^\circ\text{C}$ around this value is generally accepted, somewhat dependent on the diameter (smaller diameter tubes are more reactive [20]) and impurities or defects present on the tubes.

Figures 2 and 3 show the experimental data gathered here, from the studies mentioned above. The data are shown both as breakdown voltage V_{BD} versus length (figure 2), and breakdown power P_{BD} versus length (figure 3). Figures 2(b) and 3(b) present a ‘zoom-in’ of the data for the shorter nanotubes. Empty symbols represent the original raw data, whereas solid symbols represent the *intrinsic* breakdown power and voltage, after the power dissipated ($I_{BD}^2 R_C$) and voltage dropped ($I_{BD} R_C$) at the contacts were removed. Note the effect of removing R_C from the breakdown data, which renders the trends of V_{BD} and P_{BD} scaling to appear more clearly.

The temperature profile $T(x)$ along the SWNT during Joule heating from current flow is given by the heat conduction equation:

$$A \nabla(k \nabla T) + p' - g(T - T_0) = 0 \quad (1)$$

where $A = \pi db$ is the cross-sectional area ($b \approx 0.34 \text{ nm}$ the tube wall thickness), $k(T)$ is the SWNT thermal conductivity [21]¹, $p' = I^2 dR/dx$ is the local Joule heating rate per unit length, g is the heat loss rate to the

¹ Note that a diffusive definition of k (independent of L) is appropriate even for ‘electrically short’ SWNTs, since L refers to the separation between the electrodes, not to the physical length of the entire tube. The latter is typically longer, well over $1 \mu\text{m}$ in such experiments.

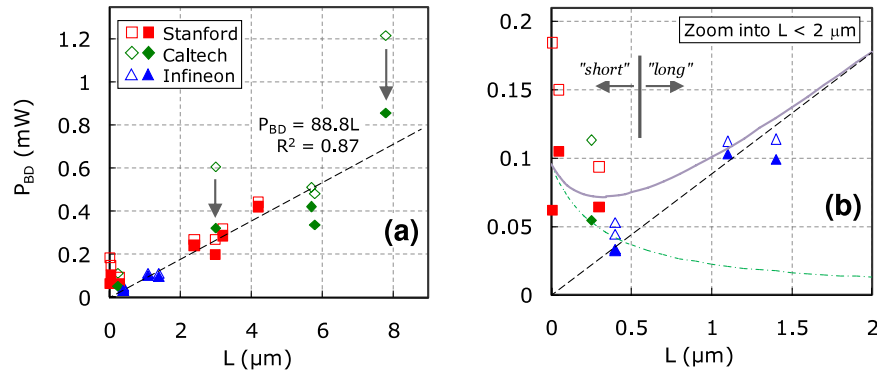


Figure 3. (a) Breakdown power versus SWNT length from the Stanford [16, 17], Caltech [15] and Infineon [14] data sets. Empty symbols are before, and solid symbols are after removing the contact power dissipation $I^2 R_C$ (arrows highlight some of the changes). (b) Same data sets, zoomed into the shorter nanotube range. Dash-dot line is the short-nanotube approximation including \mathcal{R}_T (equation (4)), dashed line is the long-nanotube approximation (equation (2)), and solid line is the solution spanning both ranges (equation (5)). The finite breakdown power at near-zero length cannot be reproduced without including the SWNT–electrode contact thermal resistance \mathcal{R}_T .

substrate and ambient per unit length, and T_0 is the ambient temperature. An explicit solution of equation (1) above does not exist because both k and p' (through the resistance R) are functions of temperature, and therefore of position along the tube. A finite-difference numerical solution computed self-consistently with the electrical resistance was provided in [15]. However, practical approximations and meaningful insight into the breakdown conditions may be obtained by assuming an average thermal conductivity and power dissipation ($p' \approx P/L$) along the nanotube. This is the approach pursued here.

For *very long* tubes, an analytical solution of the peak temperature can be written, yielding a simple, linear expression describing the breakdown power [15]:

$$P_{BD} \approx g (T_{BD} - T_0) L, \quad (2)$$

with the breakdown voltage being $V_{BD} = P_{BD}/I_{BD}$. The breakdown power P_{BD} is the power input for which the peak temperature of the SWNT (in its middle) reaches the breakdown temperature T_{BD} . Equation (2) is the ‘best-fit’ straight dashed line in figures 2 and 3, with slope $g(T_{BD} - T_0) \approx 89 \text{ W m}^{-1}$. Note this expression is independent of the thermal conductivity k , indicating that for long nanotubes the Joule heat is dissipated mostly down into the substrate, rather than laterally into their contacts (figure 1). This is in accord with the relatively flat temperature profiles calculated in figure 1(b). With the assumption of $T_{BD} = 600 \pm 100 \text{ }^\circ\text{C}$, equation (2) here yields a range for the heat sinking coefficient $g \approx 0.15 \pm 0.03 \text{ W K}^{-1} \text{ m}^{-1}$, consistent with the 0.17 value found in [15], but bearing in mind that the present study spans multiple data sets and a much wider range of SWNT diameters, substrates and lengths. This is significantly lower than the thermal conductance of radial (semi-cylindrical) heat spreading into any of the insulating substrates here alone (SiO_2 , Si_3N_4 or Al_2O_3), which is of the order $1 \text{ W K}^{-1} \text{ m}^{-1}$ or greater, indicating that heat dissipation from the nanotube is limited by the nanotube–substrate interface [15].

At the other length extreme, the simple expression above cannot be used to describe the thermal and breakdown behavior of *very short* nanotubes (figures 2(b) and 3(b)). At first glance,

an approximate solution of the heat conduction equation (2) in this length range would lead to

$$P_{BD} \approx (T_{BD} - T_0) \left(\frac{L}{8kA} \right)^{-1}, \quad (3)$$

which predicts a $1/L$ dependence of the breakdown power. However, this implies an infinitely large breakdown power (and voltage) as the nanotube length approaches zero, which is evidently *not* observed experimentally. The key to understanding the experimental data is to realize there is a finite thermal resistance (\mathcal{R}_T) associated with each of the two nanotube–electrode contacts. This yields a finite temperature drop at each contact, locally given by $\Delta T_C = T_C - T_0 = kA\mathcal{R}_T |dT_C/dx|$, as shown in figure 1(b). A more appropriate, yet simple expression of the breakdown power for very short nanotubes including this thermal contact resistance becomes

$$P_{BD} \approx (T_{BD} - T_0) \left(\frac{L}{8kA} + \frac{\mathcal{R}_T}{2} \right)^{-1}, \quad (4)$$

which is the dash-dotted line in figure 3(b), with $\mathcal{R}_T = 1.2 \times 10^7 \text{ K W}^{-1}$. This value of the nanotube–electrode thermal contact resistance is consistent with typical metal–dielectric interface thermal resistance when normalized by the small contact area here [15, 22]. This gives a finite $P_{BD} \approx 0.1 \text{ mW}$ for the shortest tubes, as their length (electrode separation) approaches zero, as seen experimentally.

At this point it is relevant to inquire what the ‘long’ and ‘short’ length scales are for the applicability of the elementary approximations above. This can be better understood by writing down a less simple, yet still analytic solution of equation (1) which includes the thermal resistance at the contacts and covers the entire length range:

$$P_{BD} = gL (T_{BD} - T_0) \times \frac{\cosh(L/2L_H) + gL_H\mathcal{R}_T \sinh(L/2L_H)}{\cosh(L/2L_H) + gL_H\mathcal{R}_T \sinh(L/2L_H) - 1} \quad (5)$$

where $L_H = (kA/g)^{1/2} \approx 0.2 \mu\text{m}$ is the characteristic thermal ‘healing’ length along the SWNT. Note this reduces

to equations (2) and (3) in [15] when $\mathcal{R}_T = 0$, and down to equations (2)–(4) above in the limits of very long and short nanotubes. This solution is plotted with the solid line in figure 3(b), showing correct asymptotic behavior in the two length limits². The ‘short-’ and ‘long-’ nanotube length range may now be thought of as compared to the order of the thermal healing length, L_H . Interestingly, these results suggest that the competing effects of heat sinking through the contacts versus the substrate yield a *minimum breakdown power* (~ 0.05 mW) of electrically-heated SWNTs in air, for tubes with length in the range $2\text{--}3L_H \approx 0.4\text{--}0.6$ μm . Nanotubes much shorter than this break down at higher power inputs following equation (4) above, whereas longer nanotubes follow the simple linear trend of equation (2). For long SWNTs it appears acceptable to neglect the thermal resistance at the electrodes (\mathcal{R}_T) altogether, as other thermal conduction pathways become dominant: mostly, from nanotube down into substrate, with thermal resistance roughly equivalent to $1/gL$ ($\sim 2 \times 10^6$ K W⁻¹ for a 3 μm SWNT, and less for longer nanotubes).

Before concluding, a number of issues must be commented on. In this simple analysis, the power dissipation ($p' = dP/dx \approx P/L$) and heat sinking (g) have been considered uniform along the nanotube. In an idealized scenario this is acceptable, as both are relatively weak functions of temperature and may be replaced with values averaged along the length of the SWNT. However, in practice they are both likely to depend of the nanotube–substrate separation. If even a small amount of ‘buckling’ is present along the nanotube, the local thermal conductance into the substrate will be severely reduced, the local resistance (and power density) of the nanotube segment will be significantly higher, and local breakdown of the SWNT may be expected. Another possibility is that of a much enhanced electric field at a buckling or defect site. Theoretical simulations have recently shown that electrostatic breakdown can occur at localized fields of the order ~ 10 V nm⁻¹ [23]. While these are much higher than the *average* axial fields caused by the lateral voltage in the data surveyed here (~ 10 V μm^{-1}), it is difficult to rule out such events at highly localized defect or buckle sites along the nanotubes. Both effects mentioned above are likely contributors to the variance seen experimentally among the different data sets for long nanotubes, even after the electrical contact effects are removed.

For short nanotubes, the probability of a buckling effect is proportionally lower, but the role of the contacts is more significant. In other words, the scatter among the breakdown data of very short SWNTs is explained by the inconsistent \mathcal{R}_T of contacts among different nanotubes, and even between the two electrodes of a single nanotube. The latter scenario will shift the peak of the temperature profile away from the middle of the nanotube [24]. A change by a factor of two in \mathcal{R}_T may alter the breakdown power of a very short SWNT by about 50% (see equation (4)). In addition to the quality of the interface, \mathcal{R}_T is also partly determined by the length of the nanotube–electrode overlap. This is usually difficult to control,

and for values below a few L_H (< 0.5 μm) the thermal contact resistance will be adversely affected. Beyond a few L_H the length of this overlap is unimportant, given the exponential drop of the temperature profile within the electrodes [25]. Finally, the diameter of the various SWNTs considered in this study also likely plays a role in their breakdown characteristics. This role is difficult to quantify unless many samples with similar diameters are systematically analyzed, but undoubtedly it controls their reactivity (here with O₂) and their ‘footprint,’ i.e. their effective heat conductance into the substrate, g . Both of these diameter effects are likely convolved within the three experimental data sets shown in figures 2 and 3.

In conclusion, this work studies in-air electrical breakdown characteristics of substrate-supported single-wall carbon nanotubes. Several published data sets were analyzed, spanning a wide range of nanotube diameters, lengths and contact properties. Nevertheless, a few simple, universal scaling rules were found to emerge, showing that the breakdown power of long nanotubes scales linearly with their length (electrode separation), whereas the breakdown of very short nanotubes is almost entirely limited by their contact resistance. The data and model show a minimum in the electrical power required to break a single-wall carbon nanotube (0.05–0.1 mW), which may be tailored through careful contact (resistance) engineering. Simple scaling models for the breakdown voltage are presented, which aid in obtaining an intuitive, physical picture of the factors limiting electrical and thermal transport, and high-voltage breakdown in substrate-supported SWNTs.

Acknowledgments

I thank Juanita Kurtin and Ali Keshavarzi at Intel for interesting discussions, which stimulated my pursuit of this problem.

References

- [1] Pop E, Mann D, Cao J, Wang Q, Goodson K E and Dai H J 2005 Negative differential conductance and hot phonons in suspended nanotube molecular wires *Phys. Rev. Lett.* **95** 155505
- [2] Yu C, Shi L, Yao Z, Li D and Majumdar A 2005 Thermal conductance and thermopower of an individual single-wall carbon nanotube *Nano Lett.* **5** 1842–6
- [3] Tseng Y-C, Phoa K, Carlton D and Bokor J 2006 Effect of diameter variation in a large set of carbon nanotube transistors *Nano Lett.* **6** 1364–8
- [4] Kim W, Javey A, Tu R, Cao J, Wang Q and Dai H 2005 Electrical contacts to carbon nanotubes down to 1 nm in diameter *Appl. Phys. Lett.* **87** 173101–3
- [5] Ouyang Y and Guo J 2006 Heat dissipation in carbon nanotube transistors *Appl. Phys. Lett.* **89** 183122–4
- [6] Prasher R 2007 Thermal conductance of single-walled carbon nanotube embedded in an elastic half-space *Appl. Phys. Lett.* **90** 143110
- [7] Qi P, Javey A, Rolandi M, Wang Q, Yenilmez E and Dai H J 2004 Miniature organic transistors with carbon nanotubes as quasi-one-dimensional electrodes *J. Am. Chem. Soc.* **126** 11774–5
- [8] Guo J *et al* 2006 Covalently bridging gaps in single-walled carbon nanotubes with conducting molecules *Science* **311** 356–9

² Recall that $\sinh(x) \sim x$ and $\cosh(x) \sim 1 + x^2/2$ as $x \rightarrow 0$. At the other extreme, $\sinh(x) = \cosh(x) = \exp(x)/2$ for $x \gg 1$.

- [9] Dean K A, Burgin T P and Chalamala B R 2001 Evaporation of carbon nanotubes during electron field emission *Appl. Phys. Lett.* **79** 1873–5
- [10] Huang N Y *et al* 2004 Mechanism responsible for initiating carbon nanotube vacuum breakdown *Phys. Rev. Lett.* **93** 075501
- [11] Hata K, Futaba D N, Mizuno K, Namai T, Yumura M and Iijima S 2004 Water-assisted highly efficient synthesis of impurity-free single-walled carbon nanotubes *Science* **306** 1362–4
- [12] Chiang I W, Brinson B E, Huang A Y, Willis P A, Bronikowski M J, Margrave J L, Smalley R E and Hauge R H 2001 Purification and characterization of single-wall carbon nanotubes (SWNTs) obtained from the gas-phase decomposition of CO (HiPco process) *J. Phys. Chem. B* **105** 8297–301
- [13] Collins P G, Arnold M S and Avouris P 2001 Engineering carbon nanotubes and nanotube circuits using electrical breakdown *Science* **292** 706–9
- [14] Seidel R V, Graham A P, Rajasekharan E, Unger E, Liebau M, Duesberg G S, Kreupl F and Hoenlein W 2004 Bias dependence and electrical breakdown of small diameter single-walled carbon nanotubes *J. Appl. Phys.* **96** 6694–9
- [15] Pop E, Mann D, Goodson K and Dai H 2007 Electrical and thermal transport in metallic single-wall carbon nanotubes on insulating substrates *J. Appl. Phys.* **101** 093710
- [16] Maune H, Chiu H-Y and Bockrath M 2006 Thermal resistance of the nanoscale constrictions between carbon nanotubes and solid substrates *Appl. Phys. Lett.* **89** 013109
- [17] Javey A, Guo J, Paulsson M, Wang Q, Mann D, Lundstrom M and Dai H J 2004 High-field quasiballistic transport in short carbon nanotubes *Phys. Rev. Lett.* **92** 106804
- [18] Collins P G, Hersam M, Arnold M, Martel R and Avouris P 2001 Current saturation and electrical breakdown in multiwalled carbon nanotubes *Phys. Rev. Lett.* **86** 3128–31
- [19] Mann D J and Hase W L 2001 Direct dynamics simulations of the oxidation of a single wall carbon nanotube *Phys. Chem. Chem. Phys.* **3** 4376–83
- [20] Chan S-P, Chen G, Gong X G and Liu Z-F 2003 Oxidation of carbon nanotubes by singlet O₂ *Phys. Rev. Lett.* **90** 086403
- [21] Pop E, Mann D, Wang Q, Goodson K E and Dai H J 2006 Thermal conductance of an individual single-wall carbon nanotube above room temperature *Nano Lett.* **6** 96–100
- [22] Lyeo H-K and Cahill D G 2006 Thermal conductance of interfaces between highly dissimilar materials *Phys. Rev. B* **73** 144301
- [23] Li C and Chou T-W 2007 Theoretical studies of the charge-induced failure of single-walled carbon nanotubes *Carbon* **45** 922–30
- [24] Mastrangelo C H, Yeh J H-J and Muller R S 1992 Electrical and optical characteristics of vacuum-sealed polysilicon microlamps *IEEE Trans. Electron Devices* **39** 1363
- [25] Durkan C, Schneider M A and Welland M E 1999 Analysis of failure mechanisms in electrically stressed Au nanowires *J. Appl. Phys.* **86** 1280–6